# Morphology Transition in Electrospinning Polymers by a Dual-Capillary System

**Fan Mei, Da-Ren Chen**

*Department of Energy, Environmental, and Chemical Engineering, Washington University, St. Louis, Missouri 63130*

Received 23 December 2008; accepted 29 June 2009
DOI 10.1002/app.31053
Published online 27 August 2009 in Wiley InterScience (www.interscience.wiley.com).

**ABSTRACT:** An experimental investigation of the fiber morphology change of fibers prepared by a dual-capillary electrospinning system, operated in the cone-jet mode, was carried out for poly(vinyl acetate) polymers of three molecular weights. The substrate morphology of the electrospun poly(vinyl acetate) could be changed significantly when the polymer's molecular weight, concentration, solvent, and outer liquid flow rate were varied. The onset of bead-to-fiber transition was determined by the critical chain overlap concentration. For solutions with a high concentration, the fiber diameter and surface were significantly affected by the physical properties of the solvents. To produce fibers of small diameter, electrospinning with a higher conductivity solution was desirable. On the other hand, a high-conductivity solution needed to be avoided to keep the fiber uniform in diameter and smooth on the surface. The comparison of electrospun fibers produced by both single-capillary and dual-capillary systems was also addressed. © 2009 Wiley Periodicals, Inc. J Appl Polym Sci 115: 204–215, 2010

**Key words:** fibers; morphology; nanotechnology

## INTRODUCTION

With electrohydrodynamic processing, one is capable of making polymers in a variety of shapes, ranging from particles to fibers, through the proper selection of the process parameters. *Electrospraying* describes a technique where particles are created, whereas the term *electrospinning* is used in situations where fibers are produced. Recently, researchers have taken notice of these techniques for their ability to create microscale and nanoscale architectures for biomedical applications, such as functional tissue scaffolds, drug-delivery carriers, patterned biochips and bioactive films/coatings, sensor development, filtration, and nanoelectronics.[1–8]

For simplicity, the point-to-plate configuration, in which a single capillary is used to feed the spray liquid from one end and the other end of the capillary serves as the point, is often used in electrospinning systems. The operational modes in a single-capillary electrospray system have been extensively investigated and summarized in the literature.[9–17] Limits of the single-capillary technique, however, exist when it is applied to complex applications. To overcome the limitations of single-capillary electrospinning, a dual-capillary electrospray technique has thus been proposed.[18–20]

Similar to electrospraying, the conventional setup for electrospinning systems typically involves only a single capillary, merely suitable for generating fibers with a particular composition in one step. However, the production of hollow fibers, coated fibers, or multicomponent fibers with submicrometer diameters is, however, limited or difficult with conventional electrospinning systems. To overcome these limitations, a number of new designs for spinnerets have recently been proposed. Among them, dual-capillary (or coaxial) spinnerets have attracted much attention. In Table I, we summarize current coaxial electrospinning studies.

There are two typical coaxial electrospinning setups.[21] In the first method, one feeds two different polymer solutions into the outer and inner spinnerets, and in the other, one uses a gas jacket to surround the electrospinning spinneret. The first kind of setup can be used to form the core–shell fiber, and the second kind of setup has the added advantage of controlling the morphology from smooth fibers to beaded fibers (or particles) without the need to vary the applied voltage. However, the operation range of the second kind of setup is limited by the gas flow rate and the size of the coaxial gas jacket.

Current research efforts have also focused on understanding the formation and morphology of

*Correspondence to:* D.-R. Chen (chen@seas.wustl.edu).
Contract grant sponsor: National Science Foundation; contract grant number: CTS-0304649.
Contract grant sponsor: Center of Nanoparticle Toxicity at the University of Rochester (funded by the Multidisciplinary University Research Initiative program of the U.S. Department of Defense).

**TABLE I**
**Summary of Coaxial-Structured Electrospinning**

| Setup | Coaxial spinneret | Gas jacket electrospinning |
|---|---|---|
| Advantage | 1. Hollow fibers can be fabricated by the removal of the core materials.<br>2. Single fibers with specific surface properties (porous or core/shell structures) can be made by postprocessing of the shell materials.<br>3. Materials normally not electrospinnable can be made into nanofibers with an electrospinnable shell material. | The gas jacket will affect the formation of the fiber morphology. |
| Disadvantage | Hollow-fiber fabrication is limited by the material properties, especially the inner and outer material solubility. | The speed of the injected gas must be controlled properly. |
| Comments | Appropriate processing parameters are desirable for fabricating specific secondary structures or new designs for employed spinnerets. | Additional modification of the spinneret may enhance the setup performance. |
| References | Sun et al.[46] Zhang et al.,[47] Li and Xia,[48] Loscertals et al.,[49] and Wang et al.[4,5] | Larsen et al.[25] and Wang et al.[4,5] |

electrospun fibers.[22–28] The morphology and diameter of electrospun fibers are dependent on a number of process parameters, including electric field strength, the flow rate of the polymer solution, and the polymer concentration. They are also affected by the polymer and solvent properties, that is, the viscosity, conductivity, and surface tension of the polymer fluid; the molecular weight; the molecular weight distribution; and the topology of the polymers.

Pham, Sharma, and Mikos[7] reviewed their predecessors' works and summarized the effect of changes in the electrospinning process parameters on the resultant fiber morphology. It has been observed that an increase in the polymer concentration (and, consequently, the viscosity) with a decrease in the surface tension favors the formation of bead-free and uniform fibers.[23,29,30] The rheological characteristics of polymer solutions also play an important role in the establishment of different regimes of beads, bead-to-fiber transitions, and complete fibers.[28,31–38]

Table II summarizes all of the studies on the morphology transition in electrospinning polymers. Most studies have focused on the effects of the solution concentration, viscosity, and molecular weight of the polymers on the morphology transition in single-capillary electrospinning systems. The formation of beads and the bead-to-fiber morphology in single-capillary electrospinning has a lot in common with the phenomenon of laminar jet breakup due to surface tension. However, regardless of whether the electrified jet consists of a viscoelastic fluid, if the Rayleigh breakup instability is not suppressed, the jet can result in a bead-to-fiber or bead-only morphology.[39–41] Researchers have also recognized the impact of elasticity on the fiber morphology in single-capillary electrospinning. A lack of elasticity of the solution prevents the formation of uniform fibers; instead, beads or bead-to-fiber structures are formed.[26,41,42]

To simply identify the bead-to-fiber range, Eda, Gupta, McKee, Shenoy, and coworkers[27,28,33–35,37] investigated morphological transitions based on critical hydrodynamic concentration, that is, the entanglement concentration ($c_e$) or critical chain overlap concentration ($c^*$). Their research described the effect of the concentration on the breakup of a polymer solution jet in terms of two critical concentrations, the initial concentration ($c_i$) and final concentration of the transition range ($c_f$). Between $c_i$ and $c_f$ is the transition bead-to-fiber range. $c_i$ is usually near $c_e$ or $c^*$. $c_e$ is a function of the entanglement molecular weight of the undiluted polymer. $c^*$ can be determined by Flory–Huggins theory.[43,44] However, although we know $c_f$ is a function of the molecular weight of polymers, we cannot mathematically determine it. Experimental results suggest that $c_f/c^*$ is typically larger than 6.0 for single-capillary electrospinning systems.[33,37]

On the basis of our survey, there is no report on the bead-to-fiber transition in a dual-capillary electrospinning system. The understanding of the solvent effects on the formation of fibers in dual-capillary setups is also very scattered. It is, thus, desirable to investigate the morphology transition in a dual-capillary electrospinning system. We are especially interested in the properties of the outer liquid, such as the volatility and conductivity, which play an important role in determining the morphology transition of the electrospun fibers. Furthermore, the understanding of the morphology changes in a dual-capillary system will help us clarify and optimize its operation.

Our main objective in this study was to investigate the formation of the electrospun fibers in a dual-capillary system, focusing on the determination of the morphology of the electrospun polymers transitioning from the bead form to the fiber.

## EXPERIMENTAL

### Setup

Figure 1 shows the dual-capillary electrospinning configuration and collection plate used in this study.

**TABLE II**
**Morphology Transition Studies of an Electrospinning System**

| Polymer/solvent | Process parameters | Comments | Reference |
|---|---|---|---|
| Amorphous PDLA and semicrystalline PLLA/DMF | Strength of the electric field, solution viscosity (e.g., concentration), charge density of the solution (by salt addition), and solution feeding rate | 1. A higher concentration and a higher charge density of the solution favor the formation of uniform nanofibers with no beadlike structure.<br>2. The diameter of the nanofibers increases with the electrospinning voltage as well as the feeding rate of the solution and decreases with the addition of the salt.<br>3. The addition of small amounts of salts or antibiotic drugs greatly changes the morphology of electrospun PDLA fibers from a bead-on-fiber structure to a uniform-fiber structure. | Zong et al.[31] |
| PS/THF PLA/DMF or DCM PEO/water | Solution entanglement number (calculated from $M_e$ in solution and $M_w$), $c$, and molecular weights | 1. With $M_e$ of undiluted PS, the electrospinning concentration regime of a PS sample of a known molecular weight can be predicted and correlated with the onset of entanglements.<br>2. Increasing $c$ or the molecular weight results in a mixture of fibers and beads. Eventually, above a certain critical values, only fibers are obtained. | Shenoy et al.[34,35] |
| PMMA/DMF | $c^*$, viscosity, molecular weight, and $c$ | 1. A plot of the zero shear viscosity with $c/c^*$ can be divided into three solution regimes: dilute ($c/c^* < 1$), semidilute and unentangled ($<1$ $c/c^* < 3$), and semidilute and entangled ($c/c^* > 3$).<br>2. Beaded fibers are initially obtained in the semidilute and unentangled regime, and uniform fibers are formed only in the semidilute and entangled regime when $c/c^*$ is greater than 6. | Gupta et al.[33] |
| Mixture of PEO and PEG/water | PEG concentrations (8–32 wt %), PEO concentrations (0.1 and 0.2 wt %), elasticity, and different PEO molecular weights | 1. All PEO and PEG mixture solutions form bead-on-fiber or uniform-fiber structures.<br>2. The presence of entanglements is not required for the formation of uniform fibers.<br>3. The fluid elasticity is the essential property controlling the morphology of the electrospun fibers. | Yu et al.[41] |
| PS/THF or DMF | $c$, $M_w$, and solvent properties | 1. Two critical concentrations, $c_i$ and $c_f$, define the morphological transition from a bead-only structure to a fiber-only structure.<br>2. $c_i$ is typically near $c_e$. The values of $c_i$ and $c_f$ decrease considerably with increasing molecular weight because of the chain entanglement effect.<br>3. The solvent has a minimal effect on the critical concentration for molecular weights higher than 100,000 g/mol.<br>4. The use of a volatile solvent may facilitate fiber formation. | Eda and Shivkumar[36,37] |
| PVA/water | $c$, [η], and $M_w$ | 1. The Berry number ([η]$c$) can be used to determine four regimes: bead-only, bead-on-fiber, fiber-only, and flat-fiber.<br>2. When the Berry number is higher than 9, a fully fibrous structure is obtained, and when it is higher than 12, the transition from round fibers to flat ribbons starts. | Tao and Shivkumar[38] |
| PLA/DCM | Gas flow rate | 1. By the use of a coaxial gas/jacket configuration to study the bead-to-fiber transition, the transition can easily be controlled by the adjustment of the gas flow rate. | Larsen et al.[25] |

[η] = intrinsic viscosity; $c$ = solution concentration; DCM = dichloromethane; DMF = *N*,*N*-dimethylformamide; $M_e$ = entanglement molecular weight; $M_w$ = weight-average molecular weight; PDLA = poly(D,L-lactic acid); PEG = poly(ethylene glycol); PEO = poly(ethylene oxide); PLA = poly(lactic acid); PLLA = poly(L-lactic acid); PMMA = poly(methyl methacrylate); PS = polystyrene; PVA = poly(vinyl alcohol); THF = tetrahydrofuran.

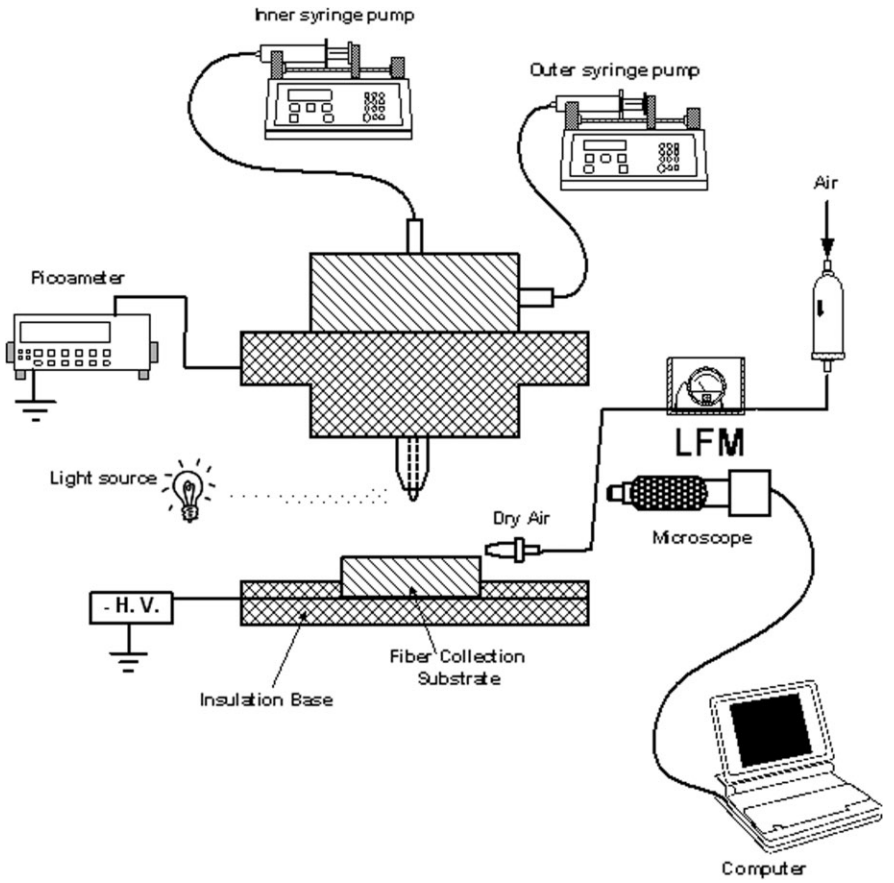


**Figure 1** Experimental setup for the synthesis of the electrospun fibers. LFM, Laminar flow meter; H.V., high voltage.

A point-to-plate arrangement with the dual-capillary tube facing the collection plate was used. The dual-capillary tube consisted of two coaxially aligned capillaries with the inside diameter of the outer capillary larger than the outside diameter of the inner capillary. Two liquid flow channels were thus formed with the coaxial capillary arrangement. The inner liquid and the outer liquid were separately injected into two flow channels by two Teflon tubes fed from two syringe pumps (Harvard model PHD 2000). Both capillaries were connected to the ground electrode, which was connected to a picoammeter (model 6485, Keithley, Hollison, MA) to measure the spray current. In this experiment, we used an inner capillary tube with an inside diameter of 0.005″ (127 μm) and an outside diameter of 0.02″ (508 μm) and an outer capillary tube with an inside diameter of 0.03″ (762 μm) and OD of 0.05″ (1270 μm). A stainless steel plate fixed on the top of a Teflon collection plate was electrified by a high-negative-voltage direct-current power supply (Bertan, model 250B-10R). The distance between the capillary and the plate was around 1.0 cm, and the applied voltage was between 4 and 7 kV.

Compressed, dry air was filtered and blown on the surface of the collection plate; this served as an additional drying process. The air flow rate used was in the range from 2 to 6 L/min and was controlled by a ball valve and measured by a laminar flow meter which is calibrated by Gilibrator.

To monitor the system electrospinning modes, viewing positions on the opposite sides of the electrospinning zone were designed. One position was for the introduction of light, and the other was for observing the shape of liquid meniscus with a microscope system, including a microscope lens (Infini-Van Video Microscope, Japan), a digital camera (model KR 222, Panasonic), a high-resolution monitor (Sony Trinitron, 1028 × 256 pixels), and a computer, to monitor and record the spinning phenomena.

Table III summarizes the physical properties of the test solvents in the experiment. The physical properties with an asterisk were measured values, and the rest of data was from Riddick et al.[45] The viscosity of the test solvents was measured by a viscometer (model SV-100 Vibro viscometer, A&D Co., Milpitas, CA). The electrical conductivity of the spray solvents was characterized by two different methods. In one method, we used a conductivity meter (Orinon 162A, Thermo Electron Corp.), and in the other method, we measured the electrical resistance with a homemade liquid cell. The other physical constants were obtained from the literature.[45]

**TABLE III**
**Physical Properties of the Solvents**

| Sample | Viscosity (cP = mPa s) | Dielectric constant | Surface tension (dyn/cm = mN/m)[a] | Density ($g/cm^3$)[a] | Conductivity ($\mu S/cm$)[a] | Boiling point (°C) |
|---|---|---|---|---|---|---|
| Ethanol (95 wt %) | 1.074 | 24.3 | 22.40 | 0.7851 | 180 | 78 |
| Acetone | 0.3371 | 20.7 (25°C) | 23.32 | 0.7899 | $4.9 \times 10^{-3}$ | 56.3 |

The data were taken from Riddick et al.[45]
[a] Measured at 20°C in the laboratory.

The surface tensions of all of the tested solvents were verified by a tensiometer (Sigma 703D, KSV Instruments, Helsinki, Finland).

The molecular weights, the corresponding intrinsic viscosity, and $c^*$ for the tested poly(vinyl acetate) (PVA) beads are given in Table IV.

### Polymer materials

McGean PVA (Cleveland, OH) beads with three different weight-average molecular weights ranging from 90,000 to 500,000 g/mol were used without further purification. Solutions were prepared by the dissolution of the polymer in acetone (HLPC grade; Sigma-Aldrich, St. Louis, MO) and 95 wt % ethanol (HLPC grade; Sigma-Aldrich).

To determine the transition concentration for each molecular weight, solutions with different concentrations were electrospun by the system shown in Figure 1. The experimental matrix studied is listed in Table V. There were four groups for each polymer weight tested. In each group, we tested at least five cases, depending on the polymer concentration in the inner solutions. The inner solution flow rate was kept at 0.5 μL/min, and the outer liquid solution flow rates varied from 1.0 μL/min to 8.0 μL/min.

## RESULTS AND DISCUSSION

### Effects of the polymer concentration on the bead-to-fiber transition

It is well known that the morphological transition from a bead-only structure to a bead-free structure takes place gradually over a range of polymer concentrations during electrospinning. In our system, we observed the transition when the outer liquid's flow rate was not lower than 3 μL/min. When the outer liquid's flow rate was lower than 3 μL/min, the tip of the capillary got clogged because of solvent evaporation and polymer buildup.

In Figures 2–4, the scanning electron microscopy (SEM) images demonstrate two extreme cases (bead-only and bead-free) and one transition (bead-to-fiber) case in the substrate morphology as a function of solution concentration for test groups 1, 5, and 9, respectively. For these three groups, the inner solvent and the outer liquid were the same: 95 wt % ethanol. The deposited substrate morphology changed gradually from the bead-only solutions (3.0 wt % for group 1, 2.0 wt % for group 5, and 1.0 wt % for group 9) to the fiber-only solutions (12.0 wt % for group 1, 10.0 wt % for group 5, and 7.5 wt % for group 9). For the same molecular weight polymer solutions, we also observed that the more viscous the solution became, the more uniform the fibers that formed were. In the bead-to-fiber transition regimes, the shape of the beads also changed from spherical to spindlelike with the increase of polymer concentration in the inner solutions. For polymer solutions with different molecular weights, the higher the molecular weight was, the narrower the transition regime was.

For groups 4, 8, and 12, we used acetone as the inner solvent and the outer liquid. As with groups 1, 5, and 9, we found the same trend of morphology change as a function of solution concentration. The

**TABLE IV**
**Physical Properties of the McGean PVA Beads**

| Grade | Molecular weight (g/mol) | Density ($g/cm^3$)[a] | Molar viscosity (cP) | $K = 1.02 \times 10^{-2}$ ($cm^3/g$), $\alpha = 0.72$[a] | | $K = 3.14 \times 10^{-2}$ ($cm^3/g$), $\alpha = 0.6$[a] | |
|---|---|---|---|---|---|---|---|
| | | | | [η] in acetone | $c^*$ (wt %)[a] | [η] in ethanol (95 wt %) | $c^*$ (wt %)[a] |
| B-15 | 90,000 | 1.19 | 10.0–12.0 | 37.6 | 2.1 | 29.5 | 2.7 |
| B-25 | 140,000 | 1.19 | 15.0–18.0 | 51.7 | 1.5 | 38.4 | 2.1 |
| B-100 | 500,000 | 1.19 | 60–75 | 129.4 | 0.6 | 82.5 | 1.0 |

[η] = intrinsic viscosity; $K$ = conductivity; α = constant; c* = weight percentage.
[a] The data were taken from Matsumoto and Ohyanagi.[32]

**TABLE V**
**Experimental Matrices of the Inner and Outer Solutions for Electrospinning**

| PVA bead | | Inner solution | Outer liquid |
|---|---|---|---|
| B-15 | Group 1 | 3.0–20.0 wt % in 95 wt % ethanol | 95 wt % ethanol |
| | Group 2 | | Acetone |
| | Group 3 | 3.0–15.0 wt % in acetone | 95 wt % ethanol |
| | Group 4 | | Acetone |
| B-25 | Group 5 | 2.0–20.0 wt % in 95 wt % ethanol | 95 wt % ethanol |
| | Group 6 | | Acetone |
| | Group 7 | 1.0–15.0 wt % in acetone | 95 wt % ethanol |
| | Group 8 | | Acetone |
| B-100 | Group 9 | 1.0–9.0 wt % in 95 wt % ethanol | 95 wt % ethanol |
| | Group 10 | | Acetone |
| | Group 11 | 1.0–9.0 wt % in acetone | 95 wt % ethanol |
| | Group 12 | | Acetone |

transition regime for the acetone groups were similar to the 95 wt % ethanol groups, ranging between 2.5–15.0 wt % for group 4, 1.5–9.0 wt % for group 8, and 1.0–7.0 wt % for group 12. Further comparisons are discussed in the next section.

### Effects of the outer liquid on the bead-to-fiber transition

Lee et al.[29] observed the reduction of irregular beads and the enhancement of electrospinning with increased *N,N*-dimethylformamide content or by using *N,N*-dimethylformamide instead of tetrahydrofuran during the electrospinning of polystyrene. An electrically good solvent, such as *N,N*-dimethylformamide, reduced the produced fiber diameter because of the increased elongational force within the solution jet. In this study, we observed that the liquid, ethanol, exhibited good solvent behavior and acetone was a poor solvent.

One of the key observations from this study was a reduction in bead formation when the inner solution (acetone as the solvent) was operated at 0.5 μL/min with a polymer (B15) concentration around 3.0 wt % and the outer liquid was switched from acetone to 95 wt % ethanol, as shown in Figure 5(A1,B1). Moreover, the fiber diameter was reduced from nearly 200 to 100 nm when the inner solution (acetone as the solvent) was operated at 0.5 μL/min with a polymer (B15) concentration of 15.0 wt % and the outer liquid was switched from acetone to 95 wt % ethanol, as shown in Figure 5(A2,B2). A similar morphology change was also observed for the cases of the polymer PVA B25 cases (shown in Fig. 6).

Moreover, by comparing the fiber-only images given in Figures 6 and 7, we found that the electrically poor solvent used as the outer liquid smoothed the fiber surface and kept the fibers uniform, whereas the electrically good solvent as the outer liquid reduced the fiber diameter. We explain these observations as follows: the 95 wt % ethanol solvent had a much higher conductivity than the acetone solvent. When ethanol was the outer liquid, it caused a higher charge density on the surface of the electrified jet during the spinning; thus, more electric charges were carried by the electrospinning jet. As the charges carried by the jet increased, higher elongation forces were imposed on the jet under the

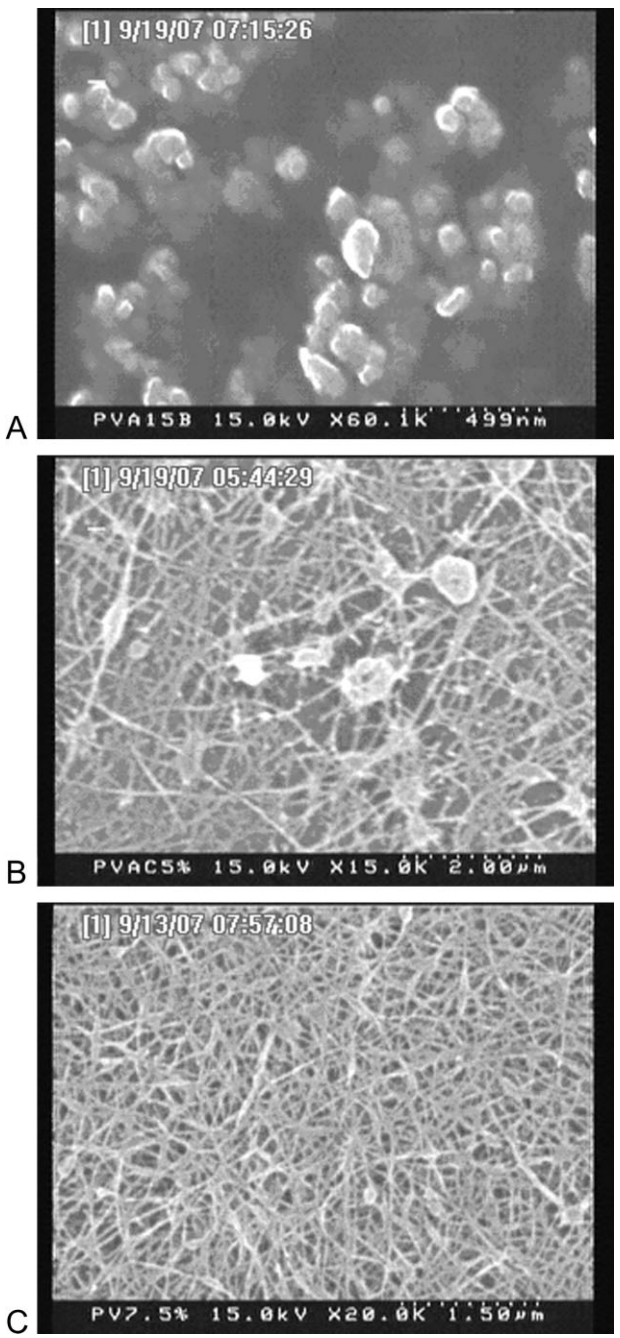


**Figure 2** SEM images for PVA (B15) polymer solutions of three different concentrations in 95 wt % ethanol (solvent): (A) 3.0, (B) 5.0, and (C) 7.5 wt %.

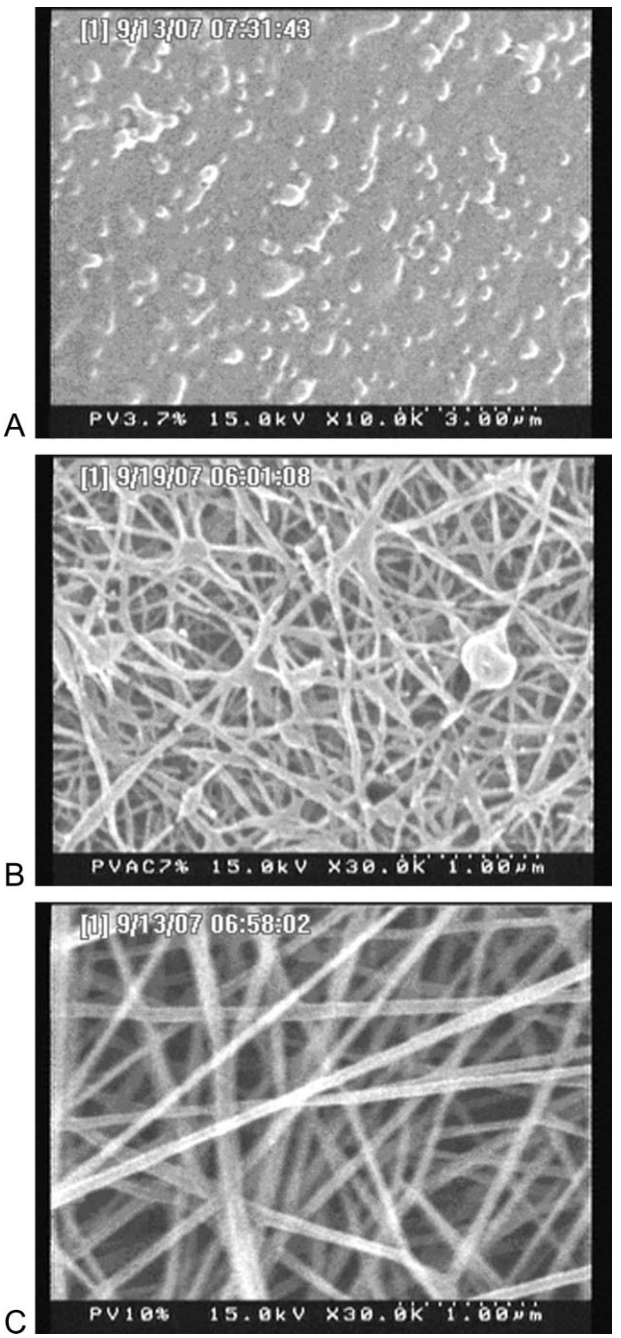


**Figure 3** SEM images for PVA (B25) polymer solutions of three different concentrations in 95 wt % ethanol (solvent): (A) 3.75, (B) 7.5, and (C) 10.0 wt %.

electrical field. It is know that the overall tension in the fibers depended on the self-repulsion of the excess charges on the jet. Thus, as the charge density increased, the beads became smaller, and the diameter of the final fibers also became substantially smaller.

To further verify our explanation, we used 95 wt % ethanol solvents with two different conductivities while 8% PVA B25 polymer–acetone was retained as the inner solution. When the outer liquid's conductivity was 10.4 μS/cm, the generated fiber's surface was smoother than the case with a conductivity of 180 μS/cm. More, the surface of the spindlelike beads shown in Figure 8(B), which had a conductivity of 79 μS/cm, was also smoother than the case shown in Figure 7(A).

### Effects of the outer liquid's flow rate on the bead-to-fiber transition

Another key observation of this study is that we could control the substrate morphology by only

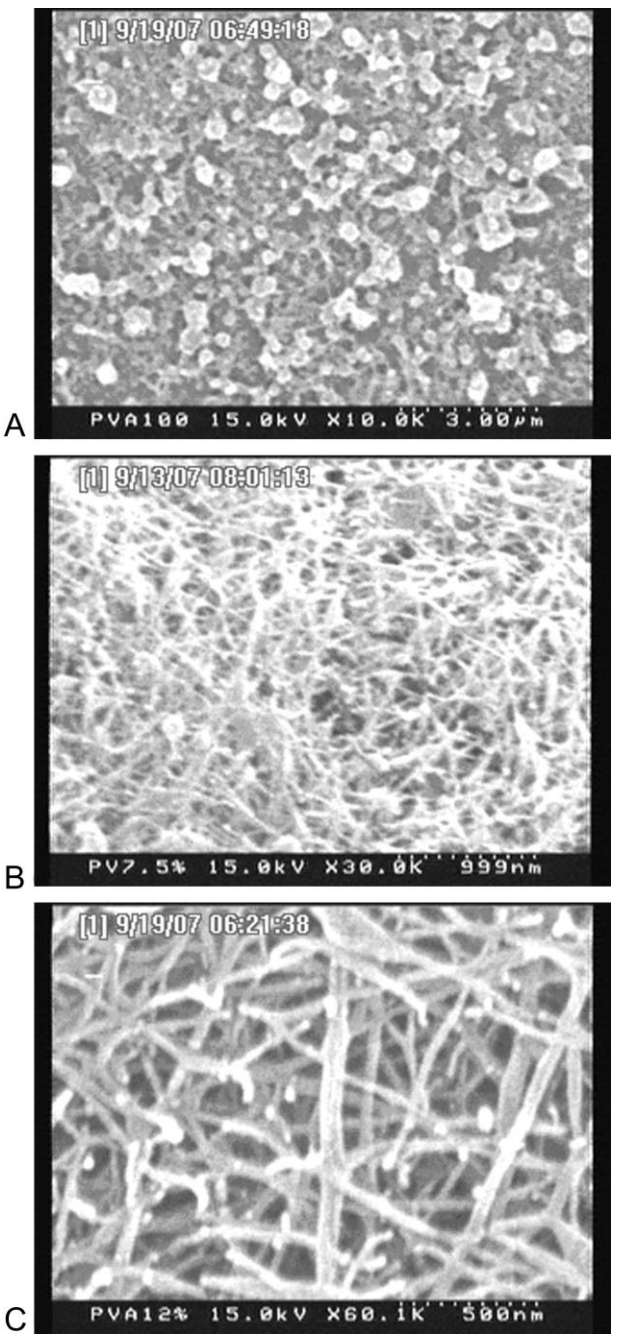


**Figure 4** SEM images for PVA (B100) polymer solutions of three different concentrations in 95 wt % ethanol (solvent): (A) 1.8, (B) 5.5, and (C) 7.5 wt %.

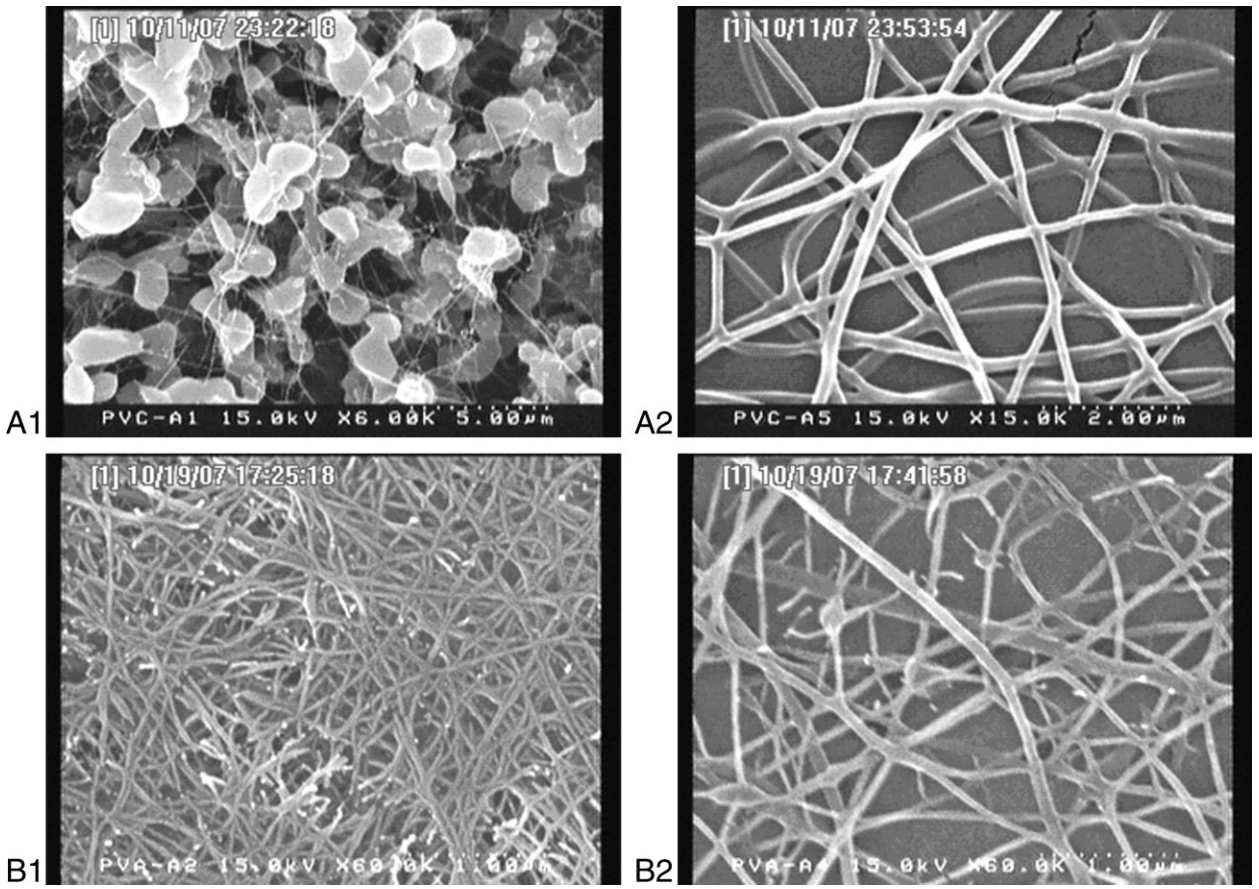


**Figure 5** SEM images for PVA (B15) polymer solutions in acetone (solvent): (A1) 3.0, (A2) 15.0, (B1) 3.0, and (B2) 15.0 wt %. The outer liquids were (A1,A2) 95 wt % ethanol and (B1,B2) acetone.

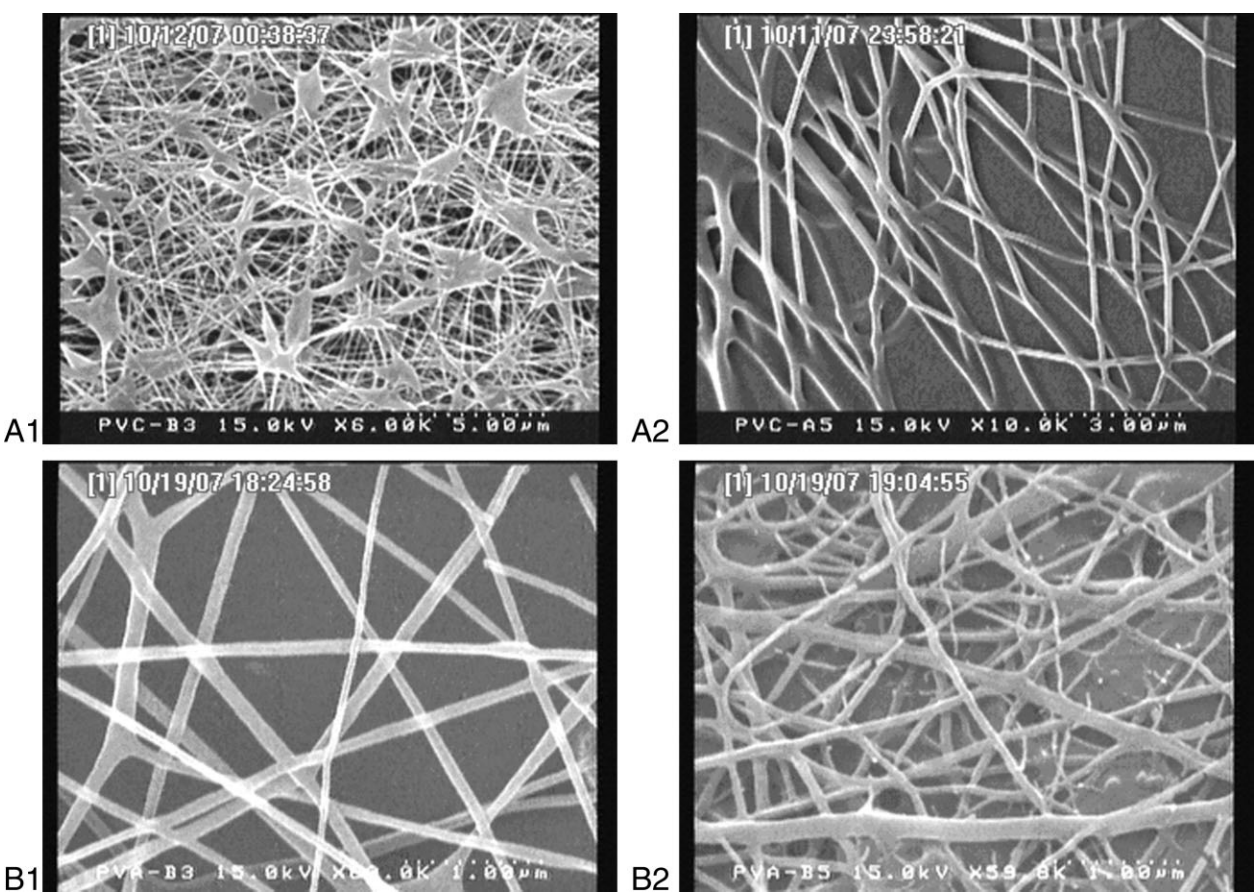


**Figure 6** SEM images for PVA (B25) polymer solutions in acetone (solvent): (A1) 3.0, (A2) 9.0, (B1) 3.0, and (B2) 9.0 wt %. The outer liquids were (A1,A2) 95 wt % ethanol and (B1,B2) acetone.

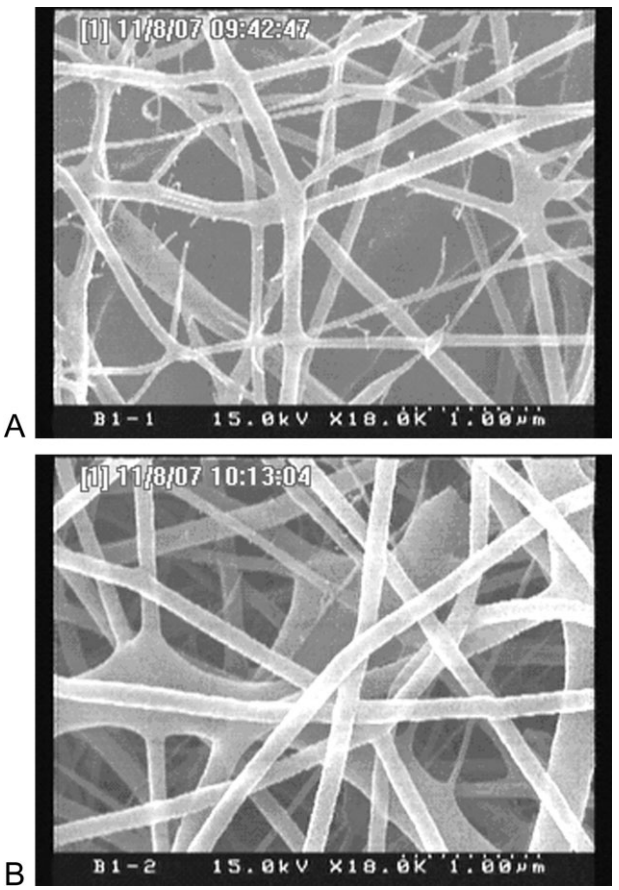


**Figure 7** SEM images for PVA (B15) polymer solutions in acetone (solvent). The outer liquid was 95 wt % ethanol with different conductivities: (A) 180.0 (9.0 wt %) and (B) 10.4 μS/cm (9.0 wt %).

varying the outer liquid's flow rate. For Figures 8 and 9, we chose a 15% PVA (B15) polymer solution as the inner solution, and the outer liquids were 95 wt % ethanol (conductivity = 79.0 μS/cm) and acetone, correspondingly. We observed that the fiber diameter decreased when we slightly increased the outer liquid's flow rate to 3.5 μL/min. When we continued increasing the outer liquid's flow rate, spindlelike beads [Fig. 8(B)] and bead-on-fiber structures [Fig. 9(B)] appeared.

As shown by a comparison of Figures 8(B) and 9(B), when we used ethanol as the outer liquid, its higher conductivity resulted in smaller beads or spindlelike beads appeared at a higher outer flow rate, as shown in Figure 8(B). With an increase in the outer liquid's flow rate to 8 μL/min, a bead-only substrate morphology was observed. Comparing Figures 8(C) and 9(C), we noticed that the particles in the latter image were more regular and spherical than those in Figure 8(C). That was because acetone had a lower boiling point and heat of vaporization than ethanol. Thus, ethanol evaporated at a much slower rate, and different evaporation rates of the solvent caused the different particle morphology.

### Comparison of a bead-to-fiber transition in single-capillary and dual-capillary electrospinning systems

In Figure 10 are summarized the bead-to-fiber transition data from Eda and Shivkumar[37] with our results for the dual-capillary system. To characterize the transition range, the figure is divided into three

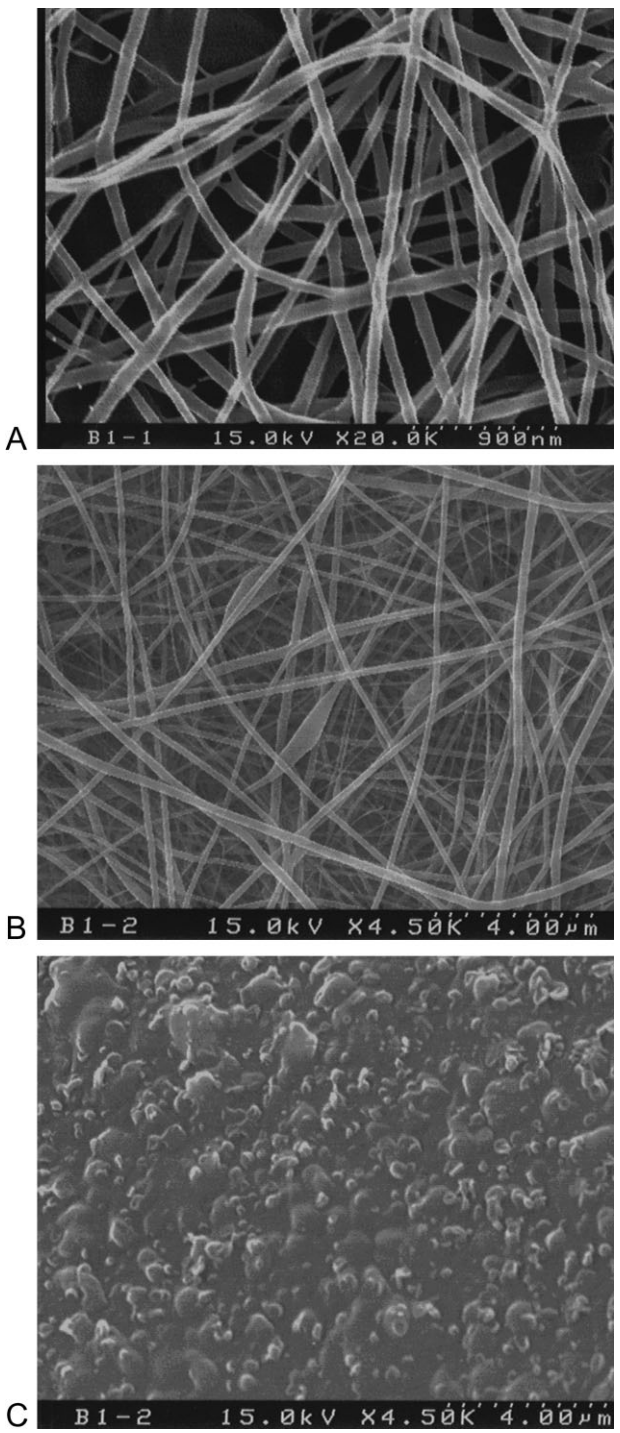


**Figure 8** SEM images for PVA (B15) polymer solutions in acetone (solvent) with different outer liquid (95 wt %) flow rates: (A) 3.5, (B) 5, and (C) 8 μL/min.

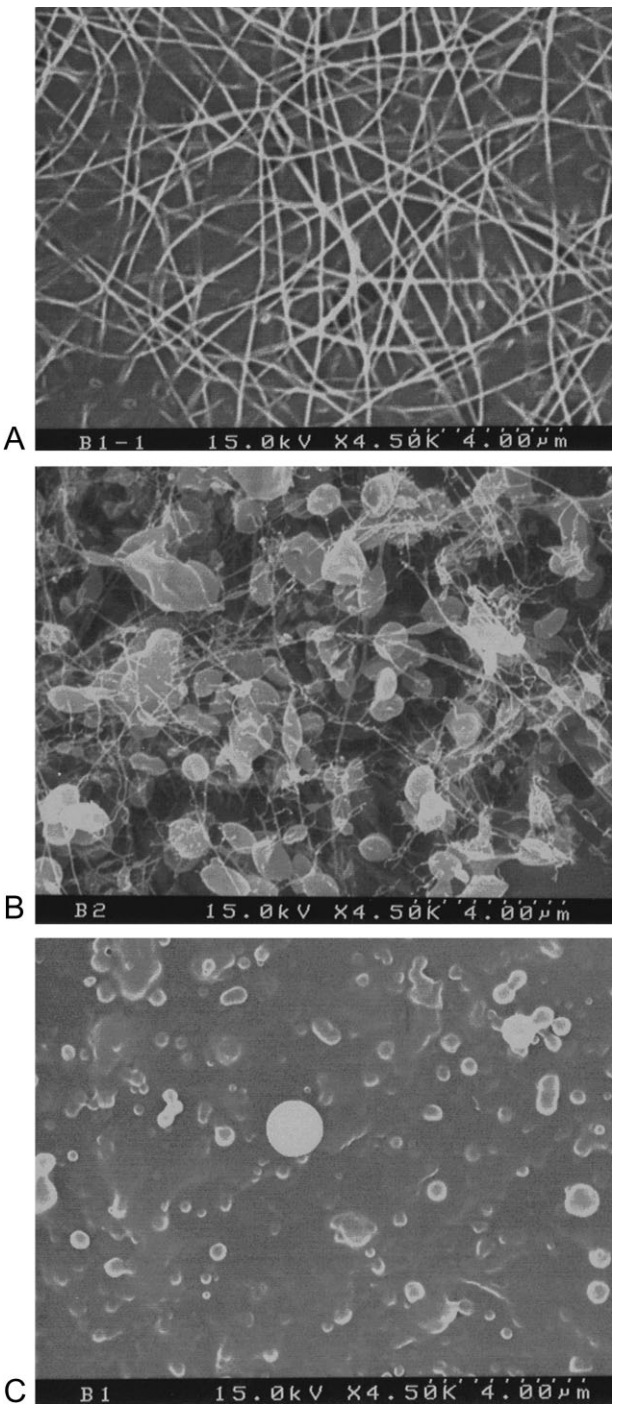


**Figure 9** SEM images for PVA (B15) polymer solutions in acetone (solvent) with different outer liquid (acetone) flow rates: (A) 3.5, (B) 5, and (C) 8 μL/min.

different regimes: the bead-only regime (identified as regime I in Fig. 10), the transition regime (regime II), and the fiber-only regime (regime III).

A comparison of the bead-to-fiber transition in the single-capillary and dual-capillary systems showed that three regimes (i.e., bead-only, transition, and fiber-only) were similar for both cases. However, the advantage of using the dual-capillary electrospinning system was that the transition regime had a similar width in the polymer molecular weight range of 100,000 g/mol.

Furthermore, we could also slightly vary the transition regime width in the dual-capillary electrospinning system. The transition regime was narrowed down when ethanol was used as the outer liquid or when we adjusted the conductivity of the outer liquid. As shown in Figure 10, when the inner/outer liquid pair was acetone/ethanol, the critical concentrations $c_i$ and $c_f$ were lower than when it was acetone/acetone. Meanwhile, when we used the same liquids in the inner and outer capillary as the solvents, the transition range followed the trend of the single-capillary system.

The other advantage for the dual-capillary electrospinning system over the single-capillary one was the unique functional characteristics of the outer liquid. When the inner and outer liquids were the same, the outer liquid compensated for the solvent evaporation loss at the capillary tip and prevented polymer clogging near the capillary tip; this made it possible to use a capillary of smaller diameter to operate appropriately. In addition, a slight increase in the outer liquid flow rate resulted in the reduction of the electrospun fiber's diameter because of the use of different flow rates for the outer and inner liquids. The different velocity profiles for the

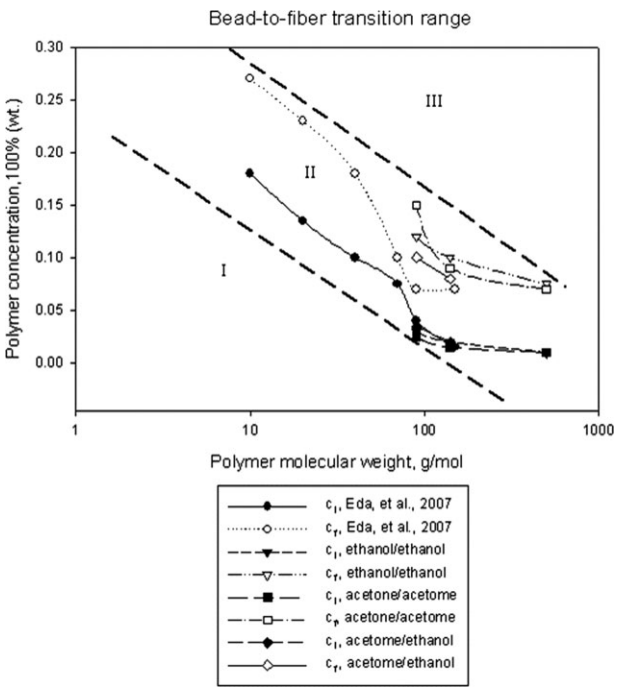


**Figure 10** Variation of $c_i$ and $c_f$ as a function of the molecular weight for the single-capillary system from Eda and Shivkumar[37] and for the dual-capillary system in this study with different inner liquid/outer liquid pairs.

inner and outer flows merged at the liquid interface, and the shear stresses in both liquids needed to be continuous at the interface. With a slight increase in the outer liquid flow rate, the shear stress change helped to trim and thin the electrospun fiber. When the outer liquid flow rate continued increasing, the mixing of the inner and outer liquids caused the polymer concentration to decrease significantly and eventually changed the spun-fiber morphology dramatically. Thus, the bead-to-fiber transition phenomenon appeared. At this point, electrospinning in the dual-capillary system acted more like it did in the single-capillary system. Moreover, when the outer liquid had a higher dielectric constant, the dual-capillary electrospinning system provided the possibility to control the jet breakup in the electrospinning process. In this study, we observed that a higher conductivity in the outer liquid (95 wt % ethanol) produced electrospun fibers of smaller diameters.

## CONCLUSIONS

The substrate morphology of the electrospun PVA depended significantly on the polymer's molecular weight, concentration, and solvent with the dual-capillary electrospinning technique. The system operational conditions also played an important role in the morphology control of electrospun polymers.

For all of the tested polymer solutions, we observed that the bead-to-fiber transition was determined solely by the inner polymer solution concentration with a fixed flow rate of outer liquid (shown in Figs. 2–4).

For PVA polymers with a molecular weight range of 90,000–500,000 g/mol, the onset of the bead-to-fiber transition could be determined by $c^*$. The observation was similar to observations in the literature for the single-capillary electrospinning system. The inner liquid solvent had a minor effect on the range of the bead-to-fiber transition. However, the fiber diameter and surface were significantly affected by the physical properties of the outer liquids. Electrospinning with a solution with a suitable conductivity produced fibers of smaller diameters. Meanwhile, higher conductivity solutions had to be avoided to keep the fiber uniform and smooth because the accumulation of electrical charges on the fiber surface caused the split of the fiber and reduced the fiber uniformity (shown in Fig. 7).

One advantage of the dual-capillary electrospinning system was the control of the substrate morphology in the bead-only, bead-on-fiber, and bead-free regimes without any change in the spun solution (i.e., inner solution). This new technique provides us with a more effective and straightforward method to produce substrates of different morphologies. Variation of the flow rate of the outer liquid not only changed the substrate morphology but also reduced the fiber diameter into the nanometer range. The other advantage of the dual-capillary electrospinning system was to vary the bead-to-fiber transition regime, which is not possible in a single-capillary electrospinning system. To narrow the transition regime, we chose a proper outer liquid, such as ethanol, and/or changed the feed flow rate and conductivity of the outer liquid.

## References


1. Boland, E. D.; Matthews, J. A.; Pawlowski, K. J.; Simpson, D. G.; Wnek, G. E.; Bowlin, G. L. Front Biosci 2004, 9, 1422.
2. Chew, S. Y.; Wen, J.; Evelyn, K.; Yim, F.; Leong, K. W. Biomacromolecules 2005, 6, 2017.
3. Chew, S. Y.; Wen, Y.; Dzenis, Y.; Leong, K. W. Curr Pharm Des 2006, 12, 4751.
4. Wang, M.; Jing, N.; Su, C. B.; Kameoka, J. Appl Phys Lett 2006, 88, 033106.
5. Wang, M.; Yu, J. H.; Kaplan, D. L.; Rutledge, G. C. Macromolecules 2006, 39, 1102.
6. Lee, J. G.; Cho, H. J.; Huh, N.; Ko, C.; Lee, W. C.; Jang, Y. H.; Lee, B. S.; Kang, I. S.; Choi, J. W. Biosens Bioelectron 2006, 21, 2240.
7. Pham, Q. P.; Sharma, U.; Mikos, A. G. Tissue Eng 2006, 12, 1197.
8. Wu, Y.; Clark, R. L. J Biomater Sci Polym Ed 2008, 19, 573.
9. Cloupeau, M.; Prunet-Foch, B. J Electrostat 1990, 25, 165.
10. Rosell-Llompart, J.; Fernandez de la Mora, J. J Aerosol Sci 1994, 25, 1093.
11. Saville, D. A. Annu Rev Fluid Mech 1997, 29, 27.
12. Higuera, F. J. J Fluid Mech 2004, 513, 239.
13. Gañán-Calvo, A. M. J Aerosol Sci 1994, 25S, 309.
14. Gañán-Calvo, A. M.; Davila, J.; Barrero, A. J Aerosol Sci 1997, 28, 249.
15. Gañán-Calvo, A. M. J Aerosol Sci 2004, 507, 203.
16. Loscertales, I. G.; Fernandez de la Mora, J. J Aerosol Sci 1993, 27, 695.
17. Fernandez de la Mora, J. Annu Rev Fluid Mech 2007, 39, 217.
18. Chen, D.; Pui, D. Y. H. U.S. Pat. 6,093,557 (2000).
19. Mei, F.; Chen, D. J Phys Fluids 2007, 19, 103303.
20. Mei, F.; Chen, D. Aerosol Air Qual Res 2008, 8, 218.
21. Teo, W. E.; Ramakrishna, S. Nanotechnology 2006, 17, R89.
22. MacDiarmid, A. G.; Jones, W. E.; Norris, I. D.; Gao, J.; Johnson, A. T.; Pinto, N. J.; Hone, J.; Han, B.; Ko, F. K.; Okuzaki, H.; Llaguno, M. Synth Met 2001, 119, 27.
23. Demir, M. M.; Yilgor, I.; Yilgor, E.; Erman, B. Polymer 2002, 43, 3303.
24. Fridrikh, S. V.; Yu, J. H.; Brenner, M. P.; Rutledge, G. C. Phys Rev Lett 2003, 90, 144502.
25. Larsen, G.; Spretz, R.; Velarde-Ortiz, R. Adv Mater 2004, 16, 166.
26. McKee, M. G.; Wilkes, G. G. L.; Colby, R. H.; Long, T. E. Macromolecules 2004, 37, 1760.
27. McKee, M. G.; Park, T.; Unal, S.; Yilgor, I.; Long, T. E. Polymer 2005, 46, 2011.
28. McKee, M. G.; Layman, J. M.; Cashion, M. P.; Long, T. E. Science 2006, 311, 353.
29. Lee, K. H.; Kim, H. Y.; Bang, H. J.; Jung, Y. H.; Lee, S. G. Polymer 2003, 44, 4029.
30. Liu, H.; Hsieh, Y.-L. J Polym Sci 2002, 40, 2119.
31. Zong, X. H.; Kim, K.; Fang, D.; Ran, S.; Hsiao, B. S.; Chu, B. Polymer 2002, 43, 4403.
32. Matsumoto, M.; Ohyanagi, Y. J Polym Sci 2003, 46, 441.

33. Gupta, P.; Elkins, C.; Long, T. E.; Wilkes, G. L. Polymer 2005, 46, 4799.
34. Shenoy, S. L.; Bates, W. D.; Frisch, H. L.; Wnek, G. E. Polymer 2005, 46, 3372.
35. Shenoy, S. L.; Bates, W. D.; Wnek, G. E. Polymer 2005, 46, 8990.
36. Eda, G. M.S. Thesis, Worcester Polytechnic Institute, 2006.
37. Eda, G.; Shivkumar, S. J Appl Polym Sci 2007, 106, 475.
38. Tao, J.; Shivkumar, S. Mater Lett 2007, 61, 2325.
39. Reneker, D. H.; Yarin, A. L.; Fong, H.; Koombhongse, S. J Appl Phys 2000, 87, 4531.
40. Zeng, J.; Hou, H.; Schaper, A.; Wendorff, J. H.; Greiner, A. e-Polymers 2003, No. 009.
41. Yu, J. H.; Fridrikh, S. V.; Rutledge, G. C. Polymer 2006, 47, 4789.
42. Theron, S. A.; Xussman, E.; Yarin, A. L. Polymer 2004, 45, 2017.
43. Flory, P. J. J Chem Phys 1941, 9, 660.
44. Huggins, M. L. J Chem Phys 1941, 9, 440.
45. Riddick, J.; Bunger, A.; William, B. Organic Solvents; 4th ed.; Wiley: New York, 1986.
46. Sun, Z. C.; Zussman, E.; Yarin, A. L.; Wendorff, J. H.; Greiner, A. Adv Mater 2003, 15, 1929.
47. Zhang, Y. Z.; Huang, Z. M.; Xu, X. J.; Lim, C. T.; Ramakrishna, S. Chem Mater 2004, 16, 933.
48. Li, D.; Xia, Y. Nano Lett 2004, 4, 933.
49. Loscertales, I. G.; Barrero, A.; Márquez, M.; Spretz, R.; Velarde-Oritz, R.; Larsen, G. J Am Chem Soc 2004, 24, 5376.